Bull. Mater. Sci., Vol. 37, No. 2, April 2014, pp. 247–255. © Indian Academy of Sciences.

Chemical bath deposition of CdS thin films doped with Zn and Cu

A I OLIVA*, J E CORONA, R PATIÑO and A I OLIVA-AVILÉS
Departamento de Física Aplicada, Centro de Investigación y de Estudios Avanzados del IPN Unidad Mérida, Km 6 Antigua Carretera a Progreso A.P. 73-Cordemex, 97310 Mérida Yucatán, Mexico

MS received 12 June 2012; revised 25 January 2013

Abstract. **Zn- and Cu-doped CdS thin films were deposited onto glass substrates by the chemical bath technique. $ZnCl_2$ and $CuCl_2$ were incorporated as dopant agents into the conventional CdS chemical bath in order to promote the CdS doping process. The effect of the deposition time and the doping concentration on the physical properties of CdS films were investigated. The morphology, thickness, bandgap energy, crystalline structure and elemental composition of Zn- and Cu-doped CdS films were investigated and compared to the undoped CdS films properties. Both Zn- and Cu-doped CdS films presented a cubic crystalline structure with (1 1 1) as the preferential orientation. Lower values of the bandgap energy were observed for the doped CdS films as compared to those of the undoped CdS films. Zn-doped CdS films presented higher thickness and roughness values than those of Cu-doped CdS films. From the photoluminescence results, it is suggested that the inclusion of Zn and Cu into CdS crystalline structure promotes the formation of acceptor levels above the CdS valence band, resulting in lower bandgap energy values for the doped CdS films.**

Keywords. **Cadmium sulfide; chemical bath deposition; doping; optical window.**

1. Introduction

Due to its suitable optical, electrical and morphological properties, cadmium sulfide (CdS) has been widely recognized as a key component of the thin film-based solar cells technology (Wu 2004; Kazmerski 2006). A semiconducting direct energy bandgap value of 2·42 eV and the ease of fabrication in thin film geometry make the CdS an ideal candidate to be used as a buffer layer on the solar cell thin film heterostructures. CdS thin films are commonly used as optical barriers for the solar radiation with the wavelength below 515 nm (Paudel *et al* 2012; Rios-Flores *et al* 2012). High solar cell efficiencies have been recently reported using CdS thin films as a part of the complex solar cell heterostructures (Romeo *et al* 2006; Repins *et al* 2008; Jackson *et al* 2011). Among the different methods for CdS thin films fabrication, the chemical bath deposition (CBD) arises as an attractive option due to its low cost, simple processing and high potential for scalability, the latter highly required for commercial applications. High film homogeneity, low electrical resistivity and high transparency in the visible region are required characteristics for the materials that are intended to be used as window layers for solar cell applications (Kim *et al* 2012). These properties are strongly dependent on film characteristics determined by the deposition process such as the grain size and the surface roughness. For example, low grain size values are commonly associated with low thickness, low roughness and high transparency. For solar cells applications, a large grain size is required in the buffer layer in order to decrease the electrical resistance that as a consequence would increase the cell's efficiency (Romeo *et al* 2006). Large grain sizes can be achieved from the deposition process or by the application of a thermal treatment after the deposition. Although, CdS is commonly reported to grow as a *n*-type semiconductor (Moualkia *et al* 2009), some reports have demonstrated *p*-type growth of CdS (Sebastian 1993). Furthermore, doping CdS films with other chemical elements during CBD process has shown to affect the resulting physicochemical properties of the doped CdS films, such as the electrical resistivity, bandgap energy and crystalline structure. Sebastian (1993) reported a decrease on CdS bandgap energy, as low as 2·0 eV, by using Cu as a doping element during CBD process. Similar results for the bandgap energy were reported by Portillo-Moreno *et al* (2006), but using different chemical reagents for CdS doping with Cu. Lee *et al* (2000) used boron as CdS doping element and reported an increase on the electrical resistance of the boron-doped CdS films. Authors also reported changes on the crystalline structure of the boron-doped CdS after carrying out an annealing process under different gas environments. To date, several elements such as aluminum (Khallaf *et al* 2008), tin (Roy and Srivastava 2006) and erbium (Dávila-Pintle *et al* 2007), have been reported to decrease the bandgap energy and electrical resistivity of CdS when they are used as doping elements. Furthermore, low tin concentrations have shown to increase the optical transmittance of tin-doped CdS films, which is desirable for optical applications (Jafari *et al* 2011).

*Author for correspondence (oliva@mda.cinvestav.mx)

Thus, the capability of controlling CdS physical properties with the doping process becomes an important issue to address in order to optimize CdS performance on the wide range of potential optical and solar applications. Here, we report on the physical properties of doped CdS thin films fabricated by CBD technique when Zn and Cu are used as doping elements. The morphology, thickness, bandgap energy, crystalline structure and elemental composition of Zn- and Cu-doped CdS thin films are investigated and correlated to Zn and Cu concentrations, respectively. The proximity of Zn and Cu to Cd in the periodic table (similar atomic radius) along with their potential doping effects on the CdS are the main drivers of the research herein presented.

2. Chemical formation

Conventional (undoped) CdS films deposition by CBD have been previously explored and a more detailed description of the methodology can be found in Herrera *et al* (2006) and Oliva-Aviles *et al* (2010). The chemical reagents used for the conventional CdS chemical bath deposition are $CdCl_2$, NH_4NO_3, KOH and $CS(NH_2)_2$ (thiourea), where the pH of the bath is controlled by the KOH concentration (Hubert *et al* 2007). The chemical process involved in CdS formation can be described by the following chemical reactions:

$$NH_4^+ + OH^- \rightarrow NH_3 + H_2O, \tag{1}$$

$$Cd^{2+} + 4NH_3 \rightarrow \left[Cd(NH_3)_4\right]^{2+}, \tag{2}$$

$$CS(NH_2)_2 + 2OH^- \rightarrow S^{2-} + CN_2H_2 + 2H_2O, \tag{3}$$

$$\left[Cd(NH_3)_4\right]^{2+} + S^{2-} \rightarrow CdS(s) + 4NH_3. \tag{4}$$

In general, the formation of CdS films is promoted by the reaction of a cadmium salt dissolved in a basic ammonium solution, see (2). According to the chemical reactions, complex ion $[Cd(NH_3)_4]^{2+}$ is deposited onto glass substrates as $Cd(OH)_2$ and further reacts with the thiourea. The addition of thiourea (3) along with controlled heating and mechanical stirring, initiates the CdS deposition onto the surface of substrates immersed within the chemical solution. For the CdS doping process, the addition of $ZnCl_2$ (Zn doping) and $CuCl_2$ (Cu doping) salts are proposed as additional steps to the conventional CdS formation process. The atomic radii of metallic Cu (0·128 nm) and Zn (0·134 nm) are very similar and lower than the radius of Cd (0·151 nm) (Greenwood and Earnshaw 1997), rendering good conditions for CdS doping process. It is then suggested that Cu^{2+} and Zn^{2+} ions would partially substitute Cd^{2+} ions into the crystalline structure of CdS, therefore promoting the CdS doping.

Thus, the additional reactions corresponding to Zn, (5) and (6), and Cu, (7) and (8), doping processes would also take place as described below:

$$Zn^{2+} + 4NH_3 \rightarrow \left[Zn\,(NH_3)_4\right]^{2+}, \tag{5}$$

$$\left[Zn\,(NH_3)_4\right]^{2+} + S^{2-} \rightarrow ZnS(s) + 4NH_3, \tag{6}$$

$$Cu^{2+} + 4NH_3 \rightarrow [Cu(NH_3)_4]^{2+}, \tag{7}$$

$$\left[Cu\,(NH_3)_4\right]^{2+} + S^{2-} \rightarrow CuS(s) + 4NH_3. \tag{8}$$

3. Experimental

In separate experiments, Zn- and Cu-doped CdS films were deposited by the CBD technique onto Corning glass substrates. The substrates were vertically immersed within the chemical bath using custom-made Teflon substrate holders, see figure 1. The chemical bath was composed of 80 ml of $CdCl_2$ (0·02 M), 200 ml of KOH (0·5 M), 80 ml of NH_4NO_3 (1·5 M) and 80 ml of $CS(NH_2)_2$ (0·2 M). The chemical solution was magnetically stirred and fixed to a temperature of 75 °C throughout the whole deposition process. $ZnCl_2$ and $CuCl_2$ solutions, both of them at a concentration of 4 mM, were used as doping agents for the CdS. The volume and ionic concentration of Zn^{2+} and Cu^{2+} along with Cd^{2+} ionic concentration used on this work are presented in table 1. The selection of the highest molar concentrations for Zn^{2+} (0·333 mM) and Cu^{2+} (0·140 mM), see table 1, was made based on preliminary experiments carried out to correlate the doping agent concentration with the degree of precipitation of Zn and Cu. It was observed that concentrations of Zn^{2+} and Cu^{2+} above 0·333 and 0·140 mM, respectively, led to an excess of doping agent precipitates, and, consequently, no further doped-CdS film deposition on the substrates. For simplicity, we will refer to the different doped-CdS samples according to the doping agent/Cd ratio shown at the last column in table 1.

Figure 1 shows the appearance of the chemical bath when Zn (figure 1a) and Cu (figure 1b) ions are introduced into the chemical bath, after the addition of thiourea. No significant changes on the chemical bath colour with respect to the yellowish colouration of the undoped CdS were observed when Zn ions were added, see figure 1(a). However, the chemical bath took on a brownish colour when Cu ions were incorporated, see figure 1(b). Five samples were prepared for each Zn- and Cu-doped bath with deposition times of 10, 20, 30, 40, 50 and 60 min. Doped CdS films presented high transparency and adherence. The intensity of the doped CdS film colour, yellowish for Zn-doped and brownish for Cu-doped films, was observed to increase with higher doping agent concentration. The morphology of the deposited films was investigated with a scanning probe microscopy (SPM, Ambios Universal) and the thickness was measured using a profilometer (Dektak 8). The bandgap energy was estimated using a spectrophotometer (StellarNet EPP-2000) with an uncertainty of 0·01 eV, in UV–Vis region. The stoichiometry of the doped CdS films was investigated by the energy dispersive spectroscopy (EDS) technique attached to a SEM (Philips XL-30). In addition, a photoluminescence (PL) technique was also carried out to obtain the levels of energy produced by the doping effect. For this aim, a 405 nm-wavelength laser with a monochromator (Scientech 9040) and a Si–PbS photodetector (Thorlabs) were used.

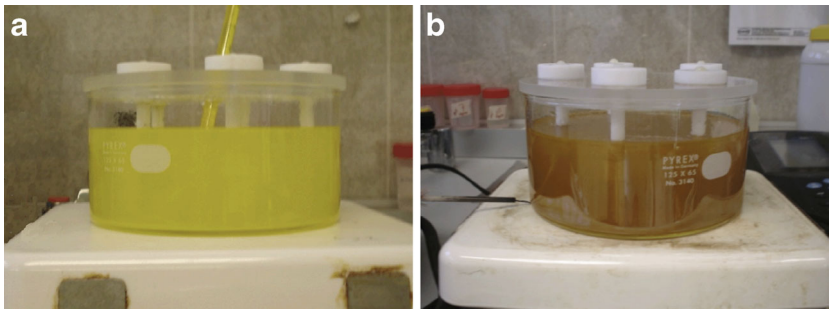

Figure 1. Colour of the chemical bath when CBD–CdS is doped with: (**a**) Zn and (**b**) Cu.

Table 1. Volumes and concentrations of Zn and Cu used for doping CdS films by CBD technique.

4 mM Zn^{2+}, V (ml)	$[Cd^{2+}]$ (mM)	$[Zn^{2+}]$ (mM)	$[Cd^{2+}]/[Zn^{2+}]$	% Zn (molar)
16	3·51	0·140	25	4
24	3·45	0·207	17	6
36	3·36	0·303	11	9
40	3·33	0·333	10	10
4 mM Cu^{2+}, V (ml)	$[Cd^{2+}]$ (mM)	$[Cu^{2+}]$ (mM)	$[Cd^{2+}]/[Cu^{2+}]$	% Cu (molar)
4	3·60	0·036	100	1
8	3·57	0·071	50	2
12	3·54	0·106	33	3
16	3·51	0·140	25	4

Finally, the crystalline structure of the doped films was studied with a X-ray diffractometer (Siemens D-5000) operating at grazing incidence with Cuα monochromatic radiation, $\lambda = 0{\cdot}15418$ nm.

4. Results

4.1 *Morphology*

Figures 2 and 3 show atomic force microscopy (AFM) micrographs of Zn- and Cu-doped CdS films respectively, at different doping agent/Cd ratios. Images of Zn- and Cu-doped CdS films correspond to deposition times of 60 and 50 min, respectively. For Zn-doped CdS films (figure 2), mean grain size values ranging from 116 to 185 nm were measured, being this range slightly lower than the one reported for undoped CdS films (150–230 nm) (Oliva *et al* 2003). On the other hand, lower values for the mean grain size, ranging from 50 to 150 nm, were observed for Cu-doped CdS films (figure 3). Figure 4 shows grain size value as a function of the dopant agent concentration.

The rms-roughness of CdS doped films was further investigated and the results are presented in figure 5. For Zn-doped CdS films (figure 5a), a low effect of the deposition time on the rms-roughness was observed as noticed from the close values obtained for all the samples fabricated at different times. A similar trend was observed for Cu-doped CdS films (figure 5b), but the rms-roughness values were significantly lower (∼3 times) respect to those of Zn-doped CdS films. Figure 5(c) shows dependence of the mean roughness value on the doping agent/CdS ratio for Zn- and Cu-doped CdS films. For a comparison, the rms-roughness value for undoped CdS films has been reported as ∼25 nm (Tec-Yam *et al* 2011) which is close to the mean values obtained for the Zn-doped CdS and higher than those of Cu-doped CdS, see figure 5(c). From the results, it can be observed that doping the CdS with Zn does not importantly affect the film roughness as compared to the undoped CdS films whereas Cu-doped films show an important decrease in their roughness. Roughness values are associated with the film thickness, which is modified during the film growth process. According to the scaling laws (Barabasi and Stanley 1995), the roughness value increases with the increase of thickness, until reaching a saturation level where no further film is deposited. This behaviour will be discussed in more detail in the next section. These results concerning the rms-roughness are in agreement with the previous discussion of the grain size results.

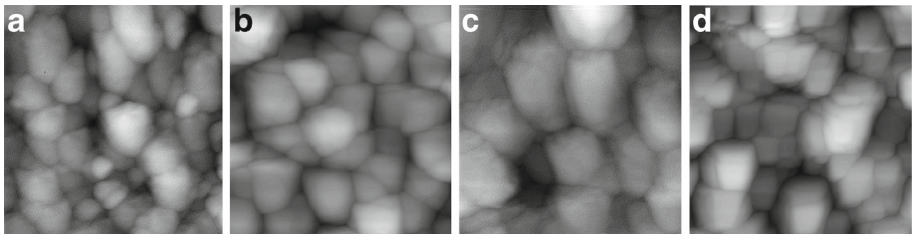

Figure 2. AFM images ($1 \times 1\ \mu m^2$) of Zn-doped CdS films at different Zn/Cd ratio: (**a**) 4%, (**b**) 6%, (**c**) 9% and (**d**) 10%. Deposition time: 60 min.

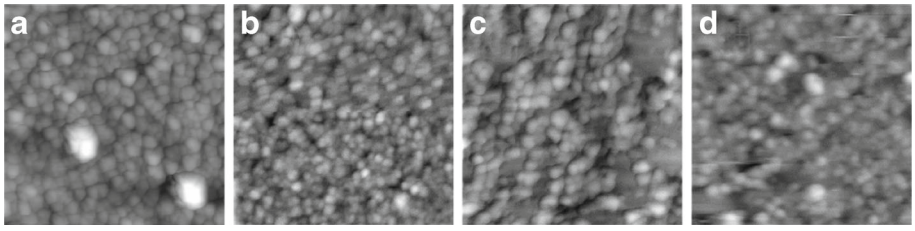

Figure 3. AFM images ($1 \times 1\ \mu m^2$) of Cu-doped CdS films at different Cu/Cd ratio: (**a**) 1%, (**b**) 2%, (**c**) 3% and (**d**) 4%. Deposition time: 50 min.

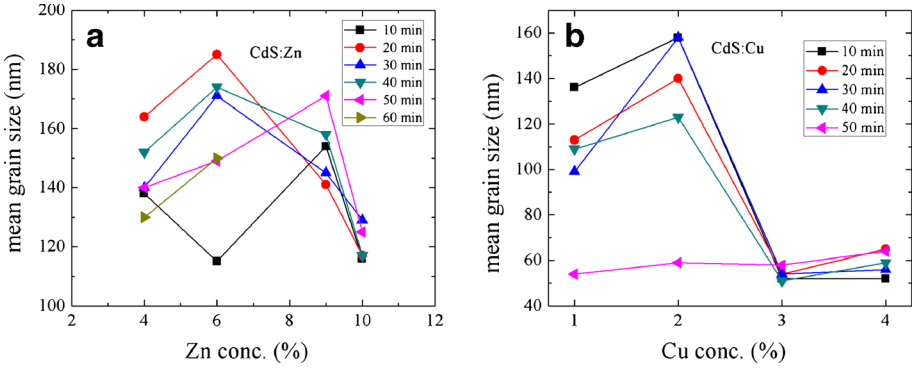

Figure 4. Mean grain size of doped-CdS films as a function of the dopant concentration for the different deposition times: (**a**) CdS:Zn and (**b**) CdS:Cu.

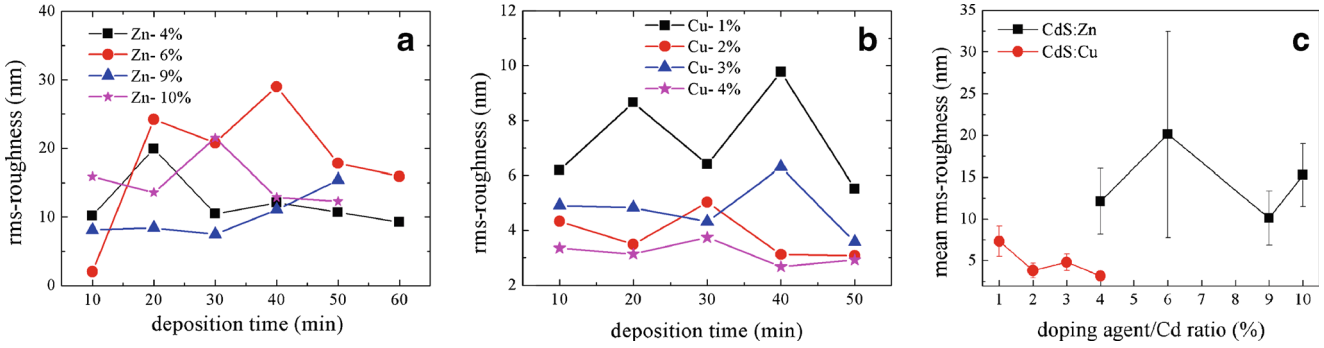

Figure 5. Surface rms-roughness of Zn- and Cu-doped CdS films. Rms-roughness vs deposition time for: (**a**) Zn-doped, (**b**) Cu-doped CdS films and (**c**) mean rms-roughness vs dopant agent/Cd ratio for Zn- and Cu-doped CdS films.

4.2 *Thickness*

Figure 6 shows thickness vs deposition time plots of Zn- and Cu-doped CdS films at different doping agent/Cd ratios. For Zn-doped CdS films, a continuous increase of the film thickness with the increase of the deposition time can be noticed up to 40 min and then the trend is inverted for longer times, see figure 6(a). The highest thickness value (∼350 nm) was registered for 9% Zn-doped CdS film, which is very similar to the maximum thickness reported for undoped CdS films fabricated under similar conditions (Tec-Yam *et al* 2011). For Cu-doped CdS films, lower thickness values were observed throughout the deposition process, see figure 6(b), being ∼90 nm the highest thickness value, registered for 1% Cu-doped film. It is suggested that the lower thickness observed for Cu-doped films can be related to the fast reaction of $CuCl_2$ when the concentration increases, producing more precipitates which results on a reduction on the film thickness.

According with scaling laws during growth (Barabasi and Stanley 1995), an increase of thickness is related with an increase of roughness before saturation, through the relation $\omega(t) \approx t^{\beta}$, where ω is the roughness, t is the deposition time and β is the growth exponent. Thus, by comparing the effect of Cu and Zn as doping agents, it is suggested that the lower thickness observed for Cu-doped films can be related to the lower solubility of the $CuCl_2$ (0·062 g/l) as compared to that of $ZnCl_2$ (4320 g/l). The lower Cu^{2+} reactivity may also inhibit the formation of CdS onto the substrates by reacting with other chemical complexes and forming undesirable precipitates resulting in a low film thickness.

4.3 *Bandgap energy*

The direct bandgap energy, E_g, was experimentally estimated from the relation $\alpha^2 = A(h\nu - E_g)$, where α is the absorption coefficient, h the Planck's constant, ν the light frequency, $h\nu$ is the energy of the incident light and A is a constant. α^2 vs $h\nu$ plots were obtained for all the doped CdS films by the spectrophotometry technique. E_g is defined as the energy value at the intersection ($\alpha^2 = 0$) of a line traced at the absorption edge at α^2 vs $h\nu$ plot (Tauc *et al* 1966). Representative plots corresponding to 10% Zn-doped and 4% Cu-doped CdS films at different fabrication times are shown in figures 7, respectively.

For Zn-doped CdS films, values of α^2 ranging between 0·5 and 1·2 can be observed at the absorption region with E_g values ranging from 2·31 to 2·39 eV, see figure 7(a). On the other hand, lower α^2 values ranging from 0·15 to 0·25 eV were measured for the Cu-doped CdS films, see figure 7(b), which is in agreement with the lower thickness observed for Cu-doped films. Furthermore, for Cu-doped films E_g values decrease with the increase of the deposition time, i.e. with film thickness from a value of 2·46 eV (10 min) to a value of 2·31 eV (50 min). The effect of increasing E_g values with the decrease of the film thickness can be explained in terms of the quantum confinement effects, which becomes more relevant for nanometric film thickness values (Glinka *et al* 2001).

It can be further observed from figures 7 that α^2 value is higher for Zn-doped films than for Cd-doped ones, being the higher values observed for Zn-doped films understood in terms of their higher film thickness as compared to that of Cd-doped films, see figure 6, according to the Beer–Lambert law (Tauc 1976). Figure 8 shows E_g values of all the doped-CdS films studied herein as a function of the deposition time. Solid and open symbols correspond to E_g values of Zn and Cu-doped CdS films, respectively. The horizontal line corresponds to the reported CdS-bulk value, 2·42 eV (Mahdi *et al* 2009) which is included as a reference. As can be observed, Zn-doped CdS films with low values of deposition time and Zn concentration present an E_g value slightly higher than that of CdS-bulk. On the other hand, in general Cu-doped CdS films show lower E_g values, as low as 2·25 eV for Cu-2% CdS ($\Delta E = 0{\cdot}17$ eV) than that of the CdS-bulk, except for low deposition times. A decrease of E_g for Cu-doped CdS films suggests the incorporation of Cu in CdS structure. A slightly higher difference on E_g value ($\Delta E = 0{\cdot}32$ eV) has been reported for Cu-doped CdS films prepared by mechanical alloying (Reyes and Velumani 2012). According to Kato *et al* (2004), doping CdS with Cu produces acceptor levels above to CdS band of valence. From

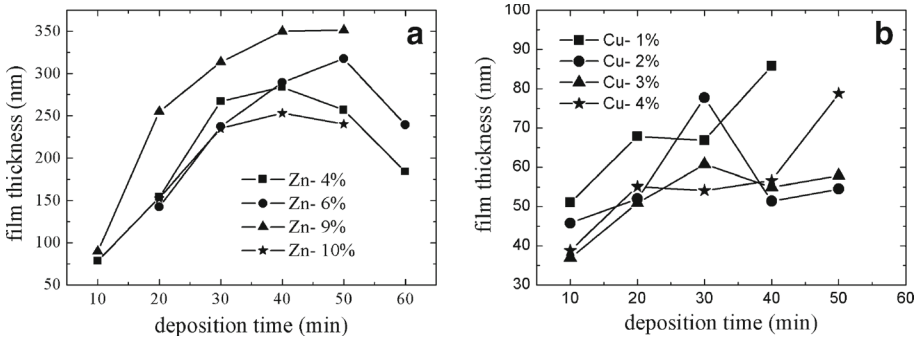

Figure 6. Thickness vs deposition time of doped CdS films at different dopant agent/Cd ratio. (**a**) Zn-doped CdS films and (**b**) Cu-doped CdS films.

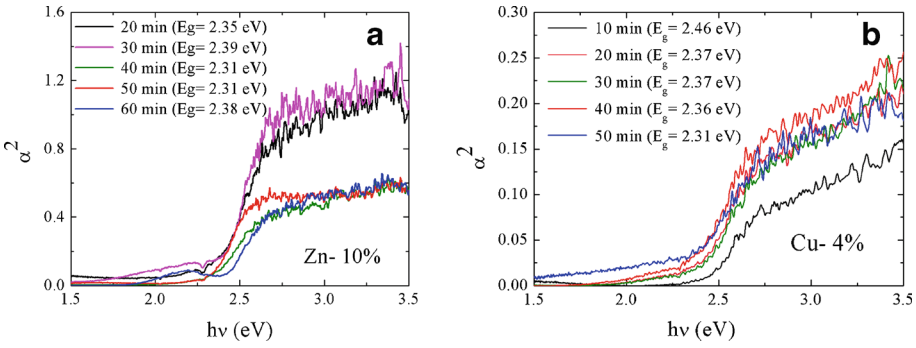

Figure 7. (colour online) α^2 vs $h\nu$ curves and energy bandgap values (E_g) for doped CdS films fabricated at different times of deposition. (**a**) Zn-10% and (**b**) Cu-4%.

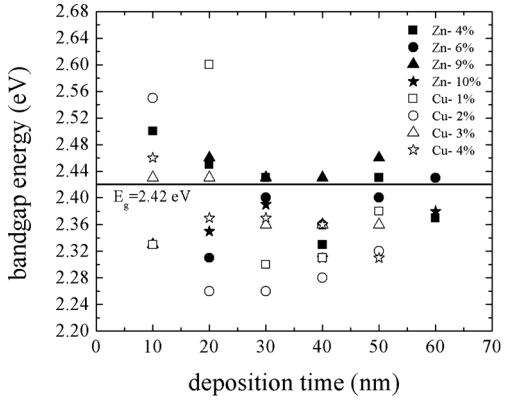

Figure 8. Bandgap energy values of Zn- and Cu-doped CdS films as measured for different deposition times and doping concentrations.

figure 8, by assuming E_g mean value for doped CdS films of 2·32 eV, the acceptor levels produced by Zn and Cu doping can be located at $\Delta E = 2{\cdot}42 - 2{\cdot}32$ eV $= 0{\cdot}1$ eV above the valence band.

4.4 *Crystalline structure*

Figure 9 shows X-ray diffractograms obtained for Zn- and Cu-doped CdS films, respectively, deposited with different concentrations during 40 min. The main (1 1 1) and the two complementary, (2 2 0) and (3 1 1), diffraction peaks confirm the hawleyite-type (cubic) structure of the doped CdS films. Sharper and thinner peaks with higher intensity were observed for Zn-doped films (figure 9a) as compared to those observed for Cu-doped films (figure 9b), suggesting this fact a larger crystallite size (CS) for Zn-doped films. According to the Scherrer relation (Cullity 1978), CS can be estimated from the diffractograms through the equation $CS = 0{\cdot}9\lambda/(\beta \cos\theta)$; where $\lambda = 0{\cdot}15418$ nm, is the X-ray wavelength provided from a Cu(α) radiation, β is the full-width at half maximum in radians and θ is the Bragg's angle. Table 2 resumes the structural data obtained for the undoped and doped CdS films. CS values for Zn- and Cu-doped CdS films obtained from the main peak (1 1 1) were estimated within the ranges of 27·7–32·8 and 25·1–28·5 nm, respectively, with CS maximum values obtained for CdS films doped with Zn-9% and Cu-2%. Data correspond to CdS films diffractograms showed in figure 9, deposited during 40 min. Reference 42-1411 from JCPDS-2002 (JCPDS-2002) for cubic CdS, reports values of the lattice parameter $a = 0{\cdot}5818$ nm and a planar distance $d = 0{\cdot}3359$ nm. From the previous discussion, it can be concluded that doping CdS with low concentrations of Zn and Cu (as used herein) slightly affects the crystalline structure of the CdS itself, which can be evidenced by the small shift of the main peaks observed for both Zn- and Cu-doped films respect to the undoped CdS films (Oliva *et al* 2001). Significant changes on the crystalline structure have been reported for Cu-doped CdS films (Shaha *et al* 2012) grown by the close space sublimation (CSS) technique along with an annealing treatment. Thus, the effect of temperature of the fabrication process plays an important role in the final crystalline structure of the doped CdS films as can be noticed by comparing the effect of CSS technique (high temperature) with the effect of CBD technique (low temperature) on the doped CdS films.

4.5 *Photoluminescence*

Photoluminescence (PL) technique was used to further investigate the doping effect on CdS films. Figure 10 shows PL intensity vs energy plots obtained for Zn-doped (10%) and Cu-doped (1%) CdS samples fabricated at a deposition time of 50 min. PL measurements were carried out at room temperature by using a laser of 405 nm-wavelength and 60 mW. It is believed that during the doping process, Zn and/or Cu atoms can be interstitially located at the crystalline lattice, substituting Cd atoms. Both Zn and Cu create donor stages near the CdS valence band which may modify the bandgap energy the CdS film. Similar PL plots were

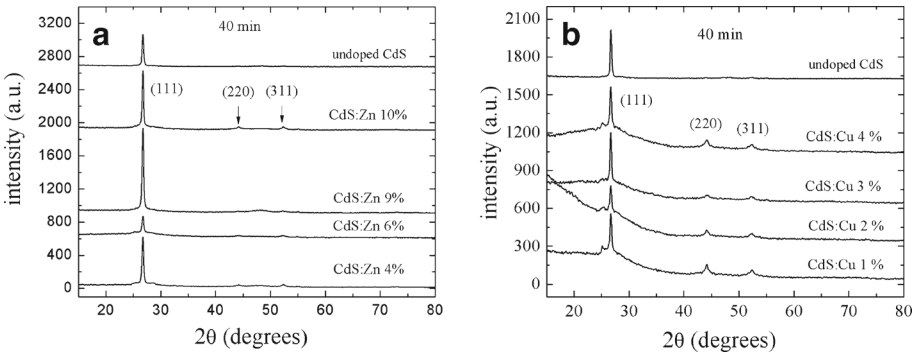

Figure 9. X-ray diffractograms of CdS films doped with different concentrations of: (**a**) Zn and (**b**) Cu. Deposition time of doped CdS films is 40 min.

Table 2. Data obtained from X-ray analysis.

Dopant conc. (%)	2θ (°)	FWHM (°)	Planar distance d (nm)	Lattice parameter a (nm)	Crystallite size, CS (nm)
Undoped CdS (40 min)					
0	26·722	0·2797	0·3336	0·5778	29·22
CdS:Zn (40 min)					
4	26·712	0·2908	0·3337	0·5780	28·10
6	26·734	0·2948	0·3334	0·5775	27·72
9	26·724	0·2755	0·3335	0·5776	29·66
10	26·728	0·2486	0·3335	0·5776	32·87
CdS:Cu (40 min)					
1	26·713	0·3100	0·3337	0·5780	26·36
2	26·704	0·2861	0·3338	0·5781	28·56
3	26·707	0·3048	0·3338	0·5781	26·81
4	26·700	0·3250	0·3338	0·5781	25·14

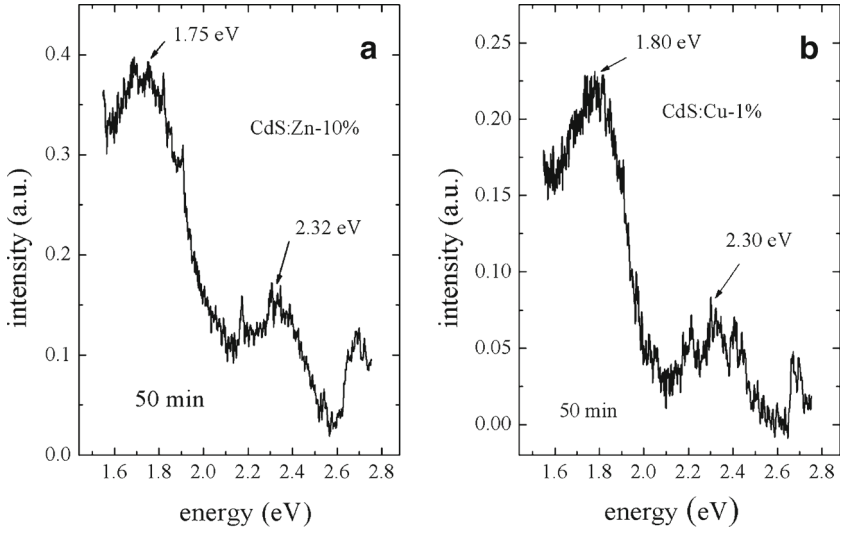

Figure 10. Room temperature PL measurements for doped CdS films deposited by chemical bath during 50 min: (**a**) Zn-doped, 10% and (**b**) Cu-doped, 1%.

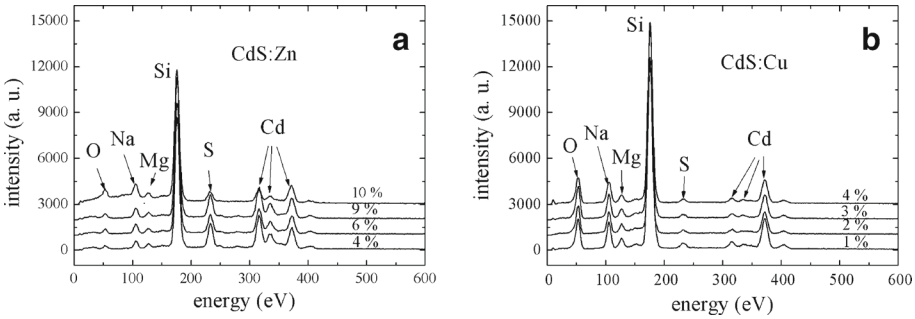

Figure 11. EDS results of deposited CdS films doped with different concentrations of: (**a**) Zn and (**b**) Cu.

Table 3. PL results and Cd/S ratio as measured for CdS films doped with Zn and Cu. Results correspond for samples deposited during 50 min.

% Zn (molar)	PL peak (E_g, eV)	PL peak (red band, eV)	Cd/S EDS ratio	% Cu (molar)	PL peak (E_g, eV)	PL peak (red band, eV)	Cd/S EDS ratio
4	2·44	1·74	1·14	1	2·30	1·80	0·86
6	2·39	1·75	1·10	2	2·35	1·78	1·08
9	2·46	1·76	1·20	3	2·36	1·77	0·86
10	2·32	1·75	0·89	4	2·35	1·76	1·00

obtained from the films doped with Zn (figure 10a) and Cu (figure 10b), where two main peaks can be observed. The peak located within the energy range of 2·30–2·32 eV corresponds to a band-to-band stage and can be associated with the bandgap energy of the corresponding film, which is in good agreement with the absorbance measurements, see figure 7. The broad peak at 1·75–1·80 eV (720–700 nm) is associated with a red band related to sulfur vacancies, as a consequence of the doping effect. Undoped CdS films do not show such a broad peak observed on the doped films, being only the bandgap energy peak observed (Osipyonok *et al* 2008). PL intensity was found to increase with the doping concentration. Table 3 summarizes PL results obtained for the different doping concentrations. Aguilar-Hernández *et al* (2006) reported PL results for CdS films deposited by close-spaced vapour transport with $CdCl_2$ annealing treatment. Authors carried out PL measurements on CdS films at low temperature (10 K), finding similar trends than those reported herein. However, they found higher intensities on the bandgap peaks and lower intensities for the red band peaks as compared to PL intensities presented in figure 10.

4.6 *Energy dispersive spectroscopy*

Figure 11 shows EDS results for Zn-doped (figure 11a) and Cu-doped (figure 11b) CdS films at different dopant agent concentration. Higher amplitudes on EDS intensities are observed for Zn-doped films, which can be explained in terms of their higher thickness as compared to Cu-doped films thickness, see figure 6. Table 3 summarizes Cd/S ratio values measured on the doped CdS films. From table 3, it can be observed that Zn-doped films grow with excess of Cd, whereas Cu-doped films mainly grow with excess of S. Due to the low dopant agent concentration, Zn and Cu peaks were not able to be captured by EDS measurements. Peaks corresponding to the glass substrate elements such as O, Na, Si and Mg were detected by EDS technique.

5. Conclusions

CdS films were doped with Zn and Cu by the chemical bath deposition technique. The effect of Zn and Cu doping concentration on the physical properties of the doped CdS films and the differences with respect to the undoped CdS films properties were investigated. Zn- and Cu-doped films presented a yellowish and brownish colour, respectively, at the macroscale. Zn-doped CdS films presented higher thickness and grain size values as compared to those values of Cu-doped films. Both Zn- and Cu-doped CdS films showed a cubic crystalline structure with (1 1 1) as the preferential orientation. Lower values and a broad range of the energy bandgap were measured for Cu-doped CdS films (2·26–2·56 eV), as compared to Zn-doped films values (2·36–2·46 eV), being the latter values similar to the undoped CdS bandgap energy value (2·42 eV). Photoluminescence results on doped CdS films suggested that the inclusion of Zn and

Cu atoms into CdS crystalline lattice promotes the formation of acceptor levels above CdS valence band, which is in agreement with the low bandgap energy values obtained for the doped-CdS films. Finally, it is suggested that the red band detected within the range of 1·75–1·80 eV on the doped films is related to the presence of sulfur vacancies, originated by the doping process.

Acknowledgements

Authors thank to Drs C Gutiérrez-Lazos and P Quintana for the fruitful discussions. Technical support of MSc Daniel Aguilar is also strongly appreciated.

References

Aguilar-Hernández J, Sartre-Hernández J, Mendoza-Perez R, Contreras-Puente G, Cárdenas-García M and Ortíz-López J 2006 *Sol. Energy Mater. Solar Cells* **90** 704

Barabasi A L and Stanley H E 1995 *Fractal concepts in surface growth* (Cambridge: Cambridge University Press)

Cullity B D 1978 *Elements of X-ray diffraction* (MA, USA: Addison-Wesley Reading)

Dávila-Pintle J A, Lozada-Morales R, Palomino-Merino M R, Rivera-Márquez J A, Portillo-Moreno O and Zelaya-Angel O 2007 *J. Appl. Phys.* **101** 013712

Glinka Y D, Lin S H, Hwang L P, Chen Y T and Tolk N H 2001 *Phys. Rev.* **B64** 085421

Greenwood N N and Earnshaw A 1997 *Chemistry of the elements* Butterworth–Heinemann. ISBN: 0080379419 2nd edn

Herrera S, Ramos C M, Patiño R, Peña J L, Cauich W and Oliva A I 2006 *Brazilian J. Phys.* **36** 1054

Hubert C, Nagavi N, Canava B, Etcheverry A and Lincot D 2007 *Thin Solid Films* **515** 6032

Jackson P, Hariskos D, Lotter E, Paetel S, Wuerz R, Menner R, Wischmann W and Powalla M 2011 *Prog. Photovolt: Res. Appl.* **19** 894

Jafari A, Zakaria A, Rizwan Z and Mohd Ghazali M S 2011 *Int. J. Mol. Sci.* **12** 6320

JCPDS 2002 International Centre for Diffraction Data. Reference 42–1411

Kato H, Sato J, Abe T and Kashiwaba Y 2004 *Phys. Status Solidi* (*C*) **1** 653

Kazmerski L L 2006 *J. Electron Spectrosc. Relat. Mater.* **150** 105

Khallaf H, Chai G, Chow L, Park S and Schulte A 2008 *J. Phys. D: Appl. Phys.* **41** 185304

Kim N H, Ryu S H, Noh H S and Lee W S 2012 *Mater. Sci. Semicond. Process* **15** 125

Lee J H, Lee Y H, Ki J H and Park Y K 2000 *Jpn. J. Appl. Phys. Part 1* **39** 1669

Mahdi M A, Kasem S J, Hassen J J, Swadi A A and Al-Ani S K J 2009 *Int. J. Nanoelectr. Mater.* **2** 163

Moualkia H, Hariech S, Aida M S, Attaf N and Laifa E L 2009 *J. Phys. D: Appl. Phys.* **42** 135404

Oliva A I, Castro-Rodriguez R, Solis-Canto O, Sosa Victor, Quintana P and Peña J L 2003 *Appl. Surf. Sci.* **205** 56

Oliva-Avilés A I, Patiño R and Oliva A I 2010 *Appl. Surf. Sci.* **256** 6090

Oliva A I, Solís-Canto O, Castro-Rodríguez R and Quintana P 2001 *Thin Solid Films* **391** 28

Osipyonok N M, Singaevsky A F, Noskov Y V, Piryatinski Y P, Smertenko P S, Dimitriev O P and Pud A A 2008 *J. Mater. Sci. Eng.* **B147** 254

Paudel N R, Wieland K A and Compaan A D 2012 *Sol. Energy Mater. Sol. Cells* **105** 109

Portillo-Moreno O *et al* 2006 *J. Electrochem. Soc.* **153** G926

Repins I, Contreras M A, Egaas B, DeHart C, Scharf J, Perkins C L, To B and Noufi R 2008 *Prog. Photovolt: Res. Appl.* **16** 235

Reyes P and Velumani F 2012 *Mater. Sci. Engg.* **B177** 1452

Rios-Flores A, Ares O, Camacho J M, Rejón V and Peña J L 2012 *Solar Energy* **86** 780

Romeo A, Khrypunov G, Kurdesau F, Arnold M, Batzner D L, Zogg H and Tiwar A N 2006 *Sol. Energy Mater. Sol. Cells* **90** 3407

Roy P and Srivastava S K 2006 *J. Phys. D: Appl. Phys.* **39** 4771

Sebastian P J 1993 *Appl. Phys. Lett.* **62** 2956

Shaha N A, Sagar R R, Mahmooda W and Syed W A A 2012 *J. Alloys Compd.* **512** 185

Tauc J J 1976 *Amorphous and liquid semiconductor* (New York: Plenum)

Tauc J J, Grigorovici R and Vancu A 1966 *Phys. Status Solidi* **15** 627

Tec-Yam S, Patiño R and Oliva A I 2011 *Current Appl. Phys.* **11** 914

Wu X 2004 *Solar Energy* **77** 803